in the literature, but there are no unambiguous examples supporting the electron-transfer mechanism for the reaction of alkylcopper–Lewis acid systems.

Finally, a possible theoretical rationale for our findings is as follows. The phenyl group, although larger than the methyl group, is a weak –I group. It therefore has an electronic preference for the outside position over the anti position, which contributes to stabilize **17(ii)** over **17(i)**. This somewhat compensates for the repulsion between the phenyl group and the nucleophile. The latter steric effect is presumably still dominant; however, the preference for the anti position is reduced by the destabilizing electronic effect. The methyl group prefers the anti position to the outside position for both steric and electronic reasons and thus occupies the anti position in preference to the phenyl group.

It is natural to ask whether a similar argument might then apply to the reaction of the *E* isomers discussed earlier. Specifically, it could be argued that structure **16(i)** (Figure 21, R = C_6H_5)) is less stable than structure **16(iii)** (R = C_6H_5), having the phenyl group inside and the methyl group anti. Indeed, the latter conformation is probably more favorable electronically. The steric preference for the anti position over the inside position, however, is very large, as can be seen in Table I. In **16(i)**, the value of ϕ is equal to −15° (see above, and Figure 21); for this value, the methyl group favors the anti position over the inside by about 3.9 kcal/mol. This preference for the less hindered position is most probably too large to be overcome by the electronic effect which should favor **16(iii)**.

Summary and Conclusion

Ab initio calculations have been carried out to study the conjugate addition of alkylcopper reagents to chiral α,β-unsaturated carbonyl compounds. We have shown that there are certain similarities to the related nucleophilic additions to carbonyl groups, particularly with regard to the steric requirements of the addition to *E* isomers. On the other hand, the electronic characteristics are quite different; the substituent effects calculated in our study are more in line with the behavior expected for *electrophilic* reactions than with the findings of calculations on other nucleophilic additions.[6,37]

Significant differences have been found between the modes of addition to *E* and *Z* isomers. In particular, the latter do not usually exhibit staggering of the C_γ substituents with respect to the forming nucleophile–C_β bond, as the Felkin–Anh model would predict. This is a consequence of the steric encumbrance of the inside position as well as the possibility of coordination of the metal center by a suitable inside substituent.

Model transition states have been deduced from our calculations, and qualitative (and in some cases quantitative) agreement has been found between the calculated and observed stereoselectivity of the addition reactions to chiral 4-alkoxy and 4-phenyl α,β-unsaturated carbonyl compounds. The transition structures for addition to the *E* isomers prefer a conformation in which the two substituents prefer the anti and inside positions, respectively. In both cases, the hydrogen atom occupies the hindered outside position. When C_γ bears an alkyl and an alkoxy group, the former takes the anti position and the latter the inside. When an alkyl and an aryl group are present, the former occupies the inside position and the latter the anti. In (*Z*)-4-alkoxy, α,β-unsaturated carbonyl compounds, the favored conformation in the transition structure has the alkyl group *outside* and the alkoxy group *inside*, since this permits coordination of the oxygen to the copper center. Finally, in (*Z*)-4-aryl α,β-unsaturated carbonyl compounds, the preferred transition structure has the aryl group outside and the methyl group anti. We believe that these models provide a realistic description of the mode of addition of alkylcopper reagents as well as other alkylmetals (including Grignard reagents) that undergo nucleophilic additions to the C=C bond of conjugated systems.

Acknowledgment. All calculations were performed at the Computer Center of the Institute for Molecular Science. A.E.D. is grateful to the Inoue Foundation for Science in Tokyo for generous financial support during his stay in Okazaki.

Chiral Discrimination and Phase Transitions in Langmuir Monolayers

David Andelman*

Contribution from the Raymond and Beverly Sackler Faculty of Exact Sciences, School of Physics and Astronomy, Tel-Aviv University, Ramat-Aviv, 69978 Tel-Aviv, Israel, and Laboratoire de Physique de la Matiere Condensée, Collège de France, 75231 Paris, Cedex 05, France. *Received September 22, 1988*

Abstract: Chiral discrimination is investigated theoretically for chiral molecules that form an insoluble Langmuir monolayer at the water/air interface. For particular tripodal shaped molecules, we calculate the chiral discrimination for various types of intermolecular interactions: van der Waals, dipoles, charges, etc. The calculation, based on Boltzmann-weighted averaging of molecular orientations, predicts a preferred heterochiral behavior for van der Waals interactions and homochiral behavior for electrostatic ones. Other interactions are also discussed. To understand monolayer phase diagrams, we draw the analogy with sublimation experiments in bulk systems and propose a three-component thermodynamic model. The variable area per molecule and also the chiral discrimination parameter enter as important parameters in the model. Phase diagrams for conglomerates and racemic compounds are calculated in qualitative agreement with experiments. Possible connections and interpretation of existing experimental data are discussed, and some new experiments for chiral monolayers are proposed.

I. Introduction

Molecules with one or more chiral centers have been studied since the nineteenth century because of their tremendous importance in many biological and organic chemical processes as well as their applications as optically active materials. Although a vast amount of knowledge has been accumulated about chiral interactions,[1] it is quite difficult to give an explanation to the origin of *chiral discrimination* and consequently predict whether a given chiral molecule interacts more favorably with its stereomeric twin

* Address correspondence to this author at Tel-Aviv University.

(1) *Optical Activity and Chiral Discrimination*; Mason, S. F., Ed.; Reidel: Dordrecht, 1979.

0002-7863/89/1511-6536$01.50/0

or with its stereomeric mirror image.

Experimentally, hundreds of natural and artificial chiral molecules have been studied.[2] Crystalline structures of pure chiral substances called *enantiomers* and of 1:1 solid mixtures of the two different enantiomers—*racemic compounds* (*racemates*)—have been identified by using crystallography techniques. Phase diagrams of the melting-point temperature as function of enantiomeric composition are also known for many chiral systems and help in the identification of chiral discrimination on a macroscopic scale.[2]

In addition, chiral molecules forming insoluble *amphiphilic monolayers* at the water/air interface have also been investigated.[3] The motivation of studying such pseudo-two-dimensional systems is the following: (i) Many of the natural phospholipids, which are the building blocks of biological cell membranes, are chiral, and their chirality is known to be of importance to the interactions of the cell membrane with proteins and other substances passing through it. (ii) Chiral molecules have complicated crystalline structure as bulk solids. It is simpler to study chiral forces at the two-dimensional water/air interface because the spacial molecular arrangement is simpler. (iii) The monolayer surface pressure is a thermodynamic variable controlling the monolayer area per molecule. Hence, the area/molecule can be varied externally. In bulk solutions, the external pressure is not a practical variable because both the solid and liquid phases are highly incompressible.

Two important types of experiments exist for chiral monolayers: using epifluorescence microscopy, various groups[4-7] have demonstrated the existence of microdomains with chiral domain boundaries in the range of few dozen micrometers. The chiral domain shapes are most probably due to a nonequilibrium growth process and are very different from the three-dimensional crystal shapes of chiral molecules having regular facetlike boundaries in accord with their crystalline space group.[2] Unfortunately, no systematic microscopy studies exist for monolayers of enantiomer mixtures as a function of enantiomeric composition.

The second type of monolayer experiments demonstrates the sensitivity of surface pressure–area isotherms to the specific stereochemistry. A chiral discrimination is found by comparing isotherms of pure enantiomeric amphiphiles with their enantiomer mixtures.[3]

The aim of the present study is to propose a simple model for chiral discrimination and phase transitions in chiral monolayers. After briefly reviewing chiral discrimination and related phase diagrams for bulk, section II, and for chiral monolayers, section III, we calculate the chiral discrimination between two tripod-shape molecules[8] in section IV. Some specific interactions are presented in section V. In section VI, we incorporate chiral interactions into a thermodynamic model for condensation and calculate the relevant monolayer phase diagrams. Finally, section VII contains further discussion of our results. Connection with experiments and some concluding remarks are given in section VIII.

II. Chiral Discrimination and Phase Diagrams of Enantiomer Mixtures

The crystallization of enantiomers and enantiomer mixtures is well documented for bulk three-dimensional systems. For an excellent review see ref 2. Melting-point phase diagrams exist for many enantiomer mixtures. The crystalline structure of different solid phases has been studied by conventional X-ray techniques. In addition, the difference between solid racemic compounds and pure enantiomers can be observed by using methods such as infrared and Raman spectroscopies.

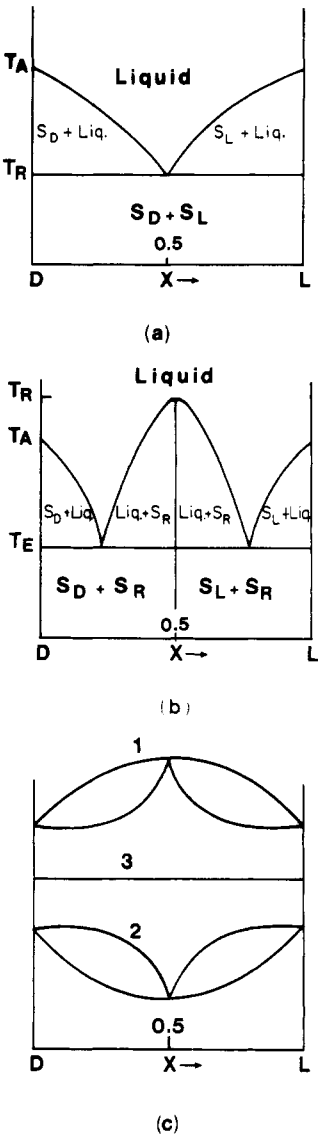

Figure 1. Melting temperature T_m as a function of the enantiomer composition, x, for (a) conglomerates, (b) racemic compound (racemates), (c) solid solutions. T_A and T_R are the melting points for pure and 1:1 enantiomer mixtures, respectively. T_E is a eutectic point. Two-phase regions between the liquid (liq), D solid (S_D), L solid (S_L), and the racemic solid (S_R) are indicated. In (c), the three possible types of solid solutions are drawn: (1) positive azeotropic point; (2) negative azeotropic point; (3) ideal solid solution.

Enantiomer mixtures are divided into three categories on the basis of their melting-point phase diagram. The three types of enantiomer mixtures are (a) *conglomerates*, (b) *racemic compounds* (*racemates*), and (c) *solid solutions*. A typical melting-point phase diagram for cases a–c is shown on Figure 1, parts a–c, respectively. We do not discuss in detail case c of solid solutions where the chiral discrimination is very weak. Only a small fraction of known chiral materials are solid solutions. For conglomerates, Figure 1a shows the melting temperature $T_m(x)$ as a function of x, the molar fraction of the two enantiomers D and L, called also the enantiomeric or racemic composition. $x = 0$ is pure D, and $x = 1$ is pure L. $T_m(x)$ varies between $T_A \equiv T_m(x=0) = T_m(x=1)$ for pure enantiomers and $T_R \equiv T_m(x=0.5)$, with $T_A \geq T_m(x) \geq T_R$. For a given composition x, below the melting point $T_m(x)$ but above T_R, the liquid coexists with a pure enantiomeric solid: liquid + S_D for $x < 0.5$, and liquid + S_L for $x > 0.5$. The point ($T = T_R$, $x = 0.5$) is an eutectic point. Since the *homochiral interactions* (HOC), D–D and L–L, are more favorable, for conglomerates, than the *heterochiral ones* (HEC),

(2) For a review see: Jacques, J.; Collet, A.; Wilen, S. H. *Enantiomers, Racemates and Resolutions*; Wiley: New York, 1981.
(3) For a review see: Stewart, M. V.; Arnett, E. M. In *Topics in Stereochemistry*; Allinger, N. L., Eliel, E. L., Wilen, S. H., Eds.; Wiley: New York, 1982.
(4) Weis, R. M.; McConnell, H. M. *Nature (London)* **1984**, *310*, 47–49.
(5) Weis, R. M.; McConnell, H. M. *J. Phys. Chem.* **1985**, *89*, 4453–4459.
(6) Heckl, W. M.; Möhwald, H. *Ber. Bunsen-Ges. Phys. Chem.* **1986**, *90*, 1159–1163.
(7) Heckl, W. M.; Lösche, M.; Cadenhead, D. A.; Möhwald, H. *Eur. Biophys. J.* **1986**, *14*, 11–17.
(8) Andelman, D.; de Gennes, P.-G. *C. R. Acad. Sci. (Paris)* **1988**, *307*(II), 233–237.

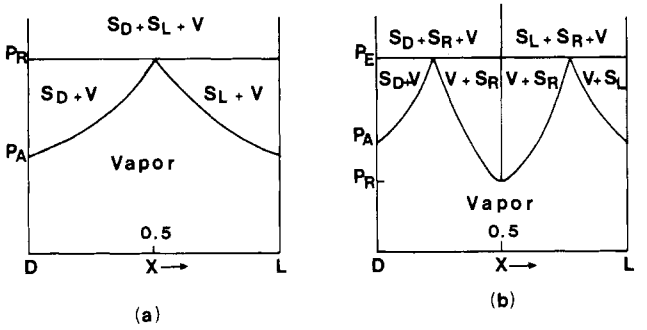

Figure 2. Sublimation pressure P_S as a function of the racemic composition, x, for conglomerates (a) and racemic compound (b). The multiphase regions between the vapor (V) and the three possible solids S_D, S_L, and S_R are indicated. P_A and P_R are the pure and the 1:1 mixture sublimation pressure, respectively. P_E is a eutectic point.

D–L, solidification is always accompanied by a full segregation of the two pure enantiomeric crystals, S_D and S_L. Hence, for $T < T_R$, the pure D crystal, S_D, coexists with the pure L crystal, S_L.

The second type of melting-point phase diagram is shown in Figure 1b and is characteristic of racemic compounds (racemates). For $x = 0.5$, the liquid solidifies at $T = T_R$ as a racemic compound—a single crystal with no optical activity. T_R can be higher (as in Figure 1b) or lower than the pure melting temperature T_A. At $T = T_E$, there are two eutectic points symmetric with respect to $x = 0.5$. Above T_E, the liquid coexists either with one of the pure solids: liquid + S_D, liquid + S_L, or with the racemate solid, liquid + S_R. Below T_E, there are two two-phase regions: $S_R + S_D$ and $S_R + S_L$. The tendency of the enantiomer mixture to form a racemic compound solid (at least in the vicinity of $x = 0.5$) is an indication that the *heterochiral* interaction D–L is preferred over the *homochiral* interactions, D–D and L–L, in contrast with conglomerates.

The third type of racemic behavior is that of solid solutions, Figure 1c. The main difference between a solid solution and the two other cases discussed above is the existence of a racemic solid over the whole range of racemic compositions, $1 \geq x \geq 0$, with $T_m(x=0.5)$ being higher (positive azeotropic point), lower (negative azeotropic point), or equal to the pure $T_m(x=0)$ (ideal solid solution). These three possibilities are shown in Figure 1c.

III. Monolayer Isotherms and Chiral Discrimination

In 1982, Stewart and Arnett[3] reviewed experimental works on phase behavior of chiral amphiphilic monolayers. Only a few experiments have been reported in the literature. The method most commonly used for detecting chiral discrimination is the measurement of the surface pressure vs the area per molecule while fixing the temperature (isotherms). This technique was invented by Langmuir[9] and is widely used for monolayers of insoluble achiral amphiphiles at the water/air interface.[10]

For relatively compressed monolayers having area/molecule in the range of a few dozen Å^2 and surface pressure in the range of few dyn/cm, a "kink" in the isotherm indicates a transition from an expanded to a more condensed phase of the monolayer. This is the so-called *liquid expanded–liquid condensed* transition. We note that the origin of the liquid expanded–liquid condensed transition is not well understood and a controversy still exists on whether this transition is a special liquid-to-liquid transition or just a liquid-to-solid one with poorly controlled environment.[11]

Chiral discrimination manifests itself as a deviation of the enantiomer mixture isotherm from the pure enantiomeric one. In particular, the *transition pressure* (the pressure where the kink in the isotherm occurs) can be plotted as a function of enantiomeric composition. Due to the very small amount of monolayer material, most of the other experimental techniques (X-rays, calorimetry) used in bulk chiral systems are much more difficult to implement for monolayers.

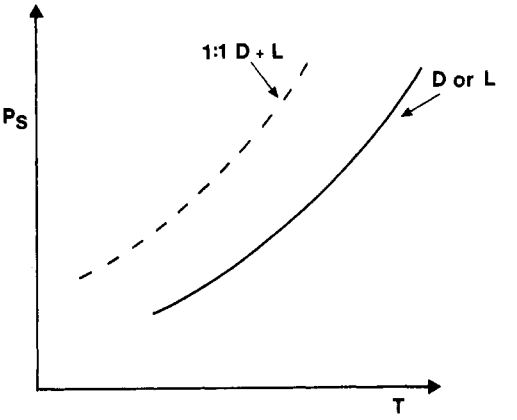

Figure 3. Sublimation pressure P_s as function of the temperature T. The solid line is for pure D or L enantiomer, while the dashed one for the 1:1 ($x = 0.5$) racemic mixture and is shifted upward with respect to the first line. Compare with Figures 1a and 2a. Only solid-to-vapor transition lines are shown.

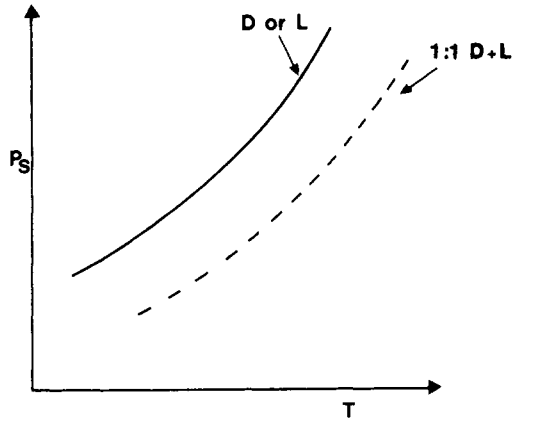

Figure 4. As in Figure 3 but the two P–T lines are inversed. Compare with Figures 1b and 2b.

An instructive way to understand phase diagrams of chiral monolayers is to draw the analogy with *sublimation* of bulk chiral systems. To the best of our knowledge, this analogy has not been previously discussed in the literature. In a sublimation experiment, the vapor phase solidifies directly without passing first through the liquid phase. The temperature as well as the external pressures can vary, contrary to the liquid–solid transition where the liquid and solid phases are quite incompressible and experiments are done at atmospheric pressure.

In Figure 2, we show schematically the sublimation pressure, $P_s(x)$, plotted against enantiomeric composition at fixed temperature.[12] Figure 2a is typical for conglomerates, while Figure 2b is typical for racemic compounds (racemate). At a fixed pressure, sublimation phase diagrams in the T–x plane look very similar to Figure 1a and 1b. The P–x and T–x phase diagrams of sublimation represent different cuts in the P–T–x parameter space. For completeness, we also show two possible phase diagrams in the P–T plane for $x = 0$ and $x = 0.5$. In Figure 3, $P_s(x=0) < P_s(x=0.5)$, while in Figure 4, $P_s(x=0) > P_s(x=0.5)$. For both cases only the gas–solid transition lines are shown.

The analogy between sublimation and monolayer experiments is quite straightforward: external pressure and specific volume

(9) Langmuir, I. *J. Am. Chem. Soc.* **1917**, *39*, 1848–1906.

(10) For a review see: (a) Gaines, G. L. *Insoluble Monolayers at Liquid Gas Interfaces*; Wiley: New York, 1966. (b) Adamson, A. W. *Physical Chemistry of Surfaces*; Wiley: New York, 1982.

(11) (a) Pallas, N. R.; Pethica, B. A. *Langmuir* **1985**, *1*, 509. (b) Middleton, S. R.; Iwasaki, M.; Pallas, N. R.; Pethica, B. A. *Proc. R. Soc. (London)* **1984**, *A396*, 143.

(12) Pages 159–165 in ref 2. For a study of vapor pressure of enantiomers and their mixtures see: Farina, M. *J. Chem. Soc., Chem. Commun.* **1987**, 1120–1121.

for the former play the role of the surface pressure and area/molecule for the latter. Thus, monolayer phase diagrams in the P–x plane should also look like Figure 2. In some of the experiments reviewed below, the whole surface pressure composition phase diagram was studied, and the identification of the chiral behavior of the monolayer, based on the analogy with sublimation, is possible. However, in several of the earlier studies only the pure and the 1:1 D + L isotherms have been obtained. With this partial information, we can identify a racemate (HEC) behavior for the cases where the 1:1 D + L transition pressure is *lower* than the enantiomeric pure one, Figure 4. Unfortunately, it is not possible to identify unambiguously the chiral behavior for the opposite case where the transition pressure for the 1:1 D + L isotherms is *higher* than for the enantiomeric pure one, Figure 3, because both conglomerates and racemates can show this relation.

Zeelen[13] in 1956 has observed a liquid expanded–liquid condensed transition for *N*-stearoyltyrosine in its pure enantiomeric form and the lack of the transition in the 1:1 L + L racemic mixture. We can argue that the transition pressure, $\Pi_c(L) = \Pi_c(D) \gg \Pi_c(D+L)$; thus, we expect a HEC (racemate) behavior as was explained above (cf. Figures 2b and 4).

More recently, Arnett et al.[14] have found for a stearamide with one chiral center (*N*-(α-methylbenzyl)stearamide) spread on an acid subphase a chiral discrimination with $\Pi_c(D+L) > \Pi_c(L)$. Here, a definite identification of the chiral behavior requires the study of the *full* phase diagram, $\Pi_c(x)$. Note that, in general, for racemates, any $\Pi_c(D+L) \neq \Pi_c(D)$ is possible, although $\Pi_c(D+L) < \Pi_c(D)$ for a strong HEC tendency.

A detailed study of a chiral lipid monolayer (*N*-myristoylalanine) has recently been published by Bouloussa and Dupeyrat.[15] Pressure–area isotherms have been measured for several mole fractions of D/L and subsequently the transition pressure Π_c has been determined as a function of the D/L mole fraction x and the temperature T. From the phase diagram, the authors concluded that the monolayer behaves as a solid solution with a positive azeotropic point (see our Figure 1c) with a HOC preference. Although we do not discuss solid solution behavior in monolayers, such a possibility exists. In bulk systems, a solid solution is an indication of a weak chiral discrimination. However, we believe that a conclusive determination of the phase behavior requires further investigation.

In a different experiment, Dvolaitzky and Guedeau[16] have observed a HEC behavior using an amphiphile with two chiral centers in the polar head group (hexadecanol–thiophosphoryl-2-phenylglycinol). The $\Pi_c(x)$ phase diagram has a minimum at $x = 0.5$ and is similar to the phase diagram of racemic compounds, our Figure 2b, in accord with their own conclusion of HEC behavior.

In summary, we would like to remark that the proposed analogy with sublimation can be useful. However, to achieve a better characterization of chiral monolayers, isotherm experiments have to be repeated over the whole range of enantiomeric composition as was done in a few studies.[15,16] Just comparing the pure with the 1:1 enantiomer mixture isotherms can often be incomplete for determining the chiral behavior.

IV. Chiral Discrimination in Langmuir Monolayers: Theory

One of the simplest examples of a chiral molecule is a *tetrahedral* (asymmetric) carbon connected to four different groups: A, B, C, and D. It is easy to see that permutations of any pair of the four groups give a new molecular configuration that is the mirror image of the original molecule. In the past, theoretical studies have used a multipole expansion of the electromagnetic forces between two tetrahedral model molecules, and the dependence of the chiral discrimination on intermolecular distance and other parameters have been calculated.[17–21]

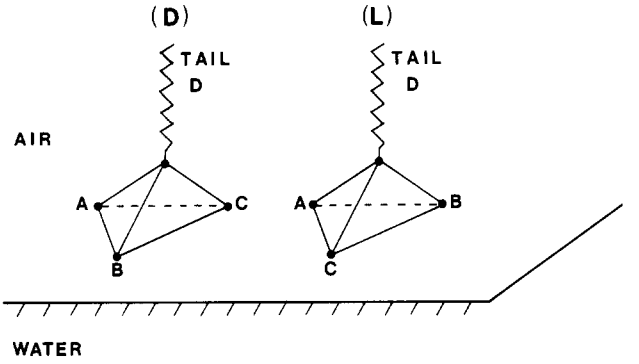

Figure 5. The two stereomeric arrangements, D and L, of the tripod amphiphile. The groups A, B, and C lie on the water/air interface and are arranged counterclockwise (clockwise) for D (L), while the group D is a hydrophobic (aliphatic) tail pointing away from the water surface.

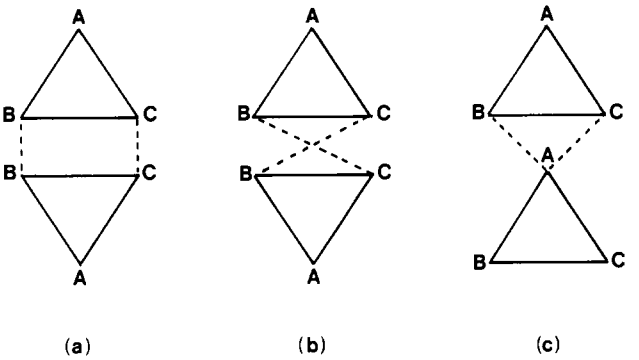

Figure 6. (a) Pair interactions between two neighbor molecules that are included in the model. In (b) and (c), two other possible interactons that are not included.

For an insoluble Langmuir monolayer, the molecules are confined on the water/air interface. We propose the following simple model[8] for a *particular* chiral amphiphile: one chiral center (e.g., a carbon or a phosphorous) connected to four different groups A, B, C, and D. Three of them, say A, B, and C, are restricted to lie on the water/air interface, while the fourth one, D, is a hydrophobic (aliphatic) chain pointing out of the water surface and into the air,[22] as is shown on Figure 5. We coined the term *tripod amphiphile*[8] for these chiral amphiphiles because they have three anchoring points on the water surface. Similar ideas about oriented triads have been used by Amaya[23] to study certain chiral association in three dimensions.

Two possible stereomers can now be constructed with such tripod molecules. The groups A, B, and C can be arranged either counterclockwise or clockwise on the water surface, while the aliphatic chain D always points up into the air. These two molecular configurations form the two different enantiomers D and L, Figure 5.

(13) Zeelen, F. J. Doctoral Thesis, State University of Leiden, Netherlands, 1956 (unpublished).
(14) (a) Arnett, E. M.; Chao, J.; Kinzig, B. J.; Stewart, M. V.; Thompson, O. *J. Am. Chem. Soc.* **1978**, *100*, 5575–5576. (b) Arnett, E. M.; Chao, J.; Kinzig, B. J.; Stewart, M. V.; Thompson, O.; Verbiar, R. J. *Ibid.* **1982**, *104*, 389–400.
(15) Bouloussa, O.; Dupeyrat, M. *Biochim. Biophys. Acta* **1988**, *938*, 395–402.
(16) Dvolaitzky, M.; Guedeau, M. A. In *Proceeding of the International Symposium on New Trends in Physics and Physical Chemistry of Polymers*; 3rd Chemical Congress of North America, Toronto, June 1988.
(17) Craig, D. P. In ref 1, p 293.
(18) Schipper, P. E. In ref 1.
(19) Schipper, P. E. *Aust. J. Chem.* **1982**, *35*, 1513–1524.
(20) (a) Schipper, D. P. *Chem. Phys.* **1977**, *26*, 29. (b) *Ibid.* **1979**, *44*, 261. (c) *Ibid*, **1981**, *57*, 105.
(21) (a) Craig, D. P.; Power, E. A.; Thirunamachardran, T. *Proc. R. Soc. (London)* **1971**, *A322*, 165. (b) Craig, D. P.; Schipper, P. E. *Ibid.* **1975**, *A342*, 19.
(22) In the model, tail–tail interactions are completely neglected. However, since the tail always points into the air, it forbids transformation of the D-tripodal base into the L one and vice versa.
(23) (a) Amaya, K. *Bull. Chem. Soc. Jpn.* **1961**, *34*, 1689–1693. (b) Amaya, K. *Ibid.* **1961**, *34*, 1803–1806. (c) Amaya, K. *Ibid.* **1962**, *35*, 1794–1797. (d) Amaya, K. *Ibid.* **1980**, *53*, 3510–3512.

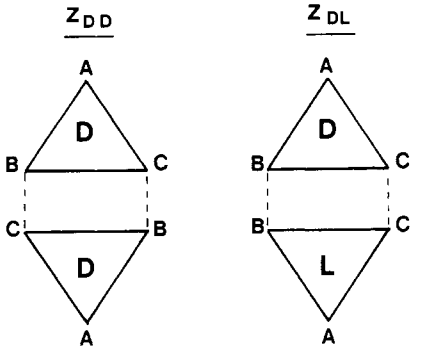

Figure 7. One of the nine orientations used to calculate Z_{DD} and Z_{DL}.

The effective interaction between a pair of tripod chiral molecules is calculated by using the following assumptions: (a) We consider interactions only between groups that are spacially the closest and neglect longer range interactions. For example, we neglect cross interactions between farther neighbors shown in Figure 6b. In a more refined calculation, the effective intermolecular interaction will depend on all pairwise interactions between the various groups of each molecular. (b) A further simplification has to do with the relative orientation of neighbor molecules. We have chosen a possible, but *certainly not unique*, "back-to-back" arrangement of the tripod molecules, Figure 6a. The advantage of such an arrangement is that it can lead to a relatively closed packing of the monolayer with a hexagonal symmetry. Another possible arrangement not included in the present model is shown in Figure 6c. In our arrangement, Figure 6a, only the three discrete 60° in-plane rotations of each molecule leaving the global orientation of the tripodal base invariant are allowed. In a more realistic calculation, the second virial coefficient (or the pair partition function as explained below) should be calculated by properly averaging over the continuum range of all possible relative orientations.

Although these assumptions are somewhat restrictive, our simple model leads to chiral discrimination in several interesting cases and may be tested experimentally. The "effective" interaction between two molecules is calculated by averaging over the internal degrees of freedom–the relative orientation of one molecule with respect to the other—with the proper Boltzmann factor. Thus, the relevant quantity to calculate is the partition function of the molecular pair: $Z_{DD} = Z_{LL}$ for a pair of the same enantiomers and $Z_{DL} = Z_{LD}$ for a pair of opposite enantiomers (cf. Figure 7). For the former, including all nine relative rotations of the pair, the partition function is

$$Z_{DD} = Z_{LL} = f_{BC}^2 + f_{AB}^2 + f_{CA}^2 + 2f_{CC}f_{AB} + 2f_{BB}f_{CA} + 2f_{AA}f_{BC} \quad (1)$$

where $f_{ij} = \exp(-V_{ij}/k_BT)$, and V_{ij} is the interaction between the two groups i, j (i, j = A, B, or C) of the two molecules; T is the temperature and k_B the Boltzmann constant. Similarly, for a pair of different enantiomers, D and L

$$Z_{DL} = Z_{LD} = f_{AA}f_{BB} + f_{BB}f_{CC} + f_{CC}f_{AA} + 2f_{AB}f_{BC} + 2f_{BC}f_{CA} + 2f_{CA}f_{AB} \quad (2)$$

The chiral discrimination parameter is conveniently defined as $\Delta = Z_{DD} - Z_{DL}$. From (1) and (2)

$$\Delta = f_{BC}^2 + f_{AB}^2 + f_{CA}^2 - f_{AA}f_{BB} - f_{BB}f_{CC} - f_{CC}f_{AA} + 2f_{CC}f_{AB} + 2f_{BB}f_{CA} + 2f_{AA}f_{BC} - 2f_{AB}f_{BC} - 2f_{BC}f_{CA} - 2f_{CA}f_{AB} \quad (3)$$

Depending on the sign of Δ, two cases are distinguished: if $\Delta > 0$, the homochiral interactions, D–D and L–L, are larger than the heterochiral one, D–L, and there is a tendency for chiral segregation. This is the homochiral case (HOC). On the other hand, $\Delta < 0$ is the heterochiral case (HEC), where chiral segregation is disfavored. We discuss now some specific examples where the intergroup interactions V_{ij} can be electrostatic (charge–charge or dipole–dipole), van der Waals, hydrogen bonding, etc.

V. Chiral Discrimination: Specific Interactions

1. Free Rotating Limit: High Temperatures. In the limit of high temperatures, $V_{ij} \ll k_BT$, including only first-order terms in V_{ij}, we get from (3) $\Delta = 0$. This is the free rotating limit for which the model does not show a chiral discrimination. In a previous study, Salem et al.[24] have shown for the free rotating limit that a chiral discrimination between two tetrahedral molecules allowed to rotate in three dimensions does not exist if only two-body interactions are considered. A small discrimination arises if six-body or higher interactions are included; for example, if three of the four groups of the first molecule interact simultaneously with three groups of the second molecule. However, such high-order corrections lie beyond the scope of the present paper. Chiral discrimination exists in our model even for two-body interactions but *not* in the special free-rotating limit.

2. van der Waals Interactions. Here all intermolecular interactions between the groups are dispersion-type like van der Waals interactions:

$$V_{ij} = -M\alpha_i\alpha_j \quad (4)$$

where $\alpha_i = \alpha_A$, α_B, or α_C is the polarizability of the group i and M is a prefactor. We show below that our model always predicts $\Delta < 0$ (HEC) for van der Waals interaction, *regardless of the values of* α_A, α_B, and α_C, as long as they differ one from another. If any two of the α's are equal, the tripod is no longer chiral; hence $\Delta = 0$. This general result for van der Waals interactions is tightly connected to the fact that V_{ij} in (4) depends only on the *product* of α_i and α_j.

Though not able to prove analytically the inequality $\Delta \leq 0$, we have verified it numerically for numerous values of α_A, α_B, and α_C. We also have proved it analytically for several more restricted cases: (i) $\Delta = 0$ whenever two of the three α_i's are equal; (ii) high-temperature expansion up to third order in $1/T$

$$\Delta \simeq -\tfrac{1}{2}(M/k_BT)^3(\alpha_A - \alpha_B)^2(\alpha_B - \alpha_C)^2(\alpha_C - \alpha_A)^2 \leq 0 \quad (5)$$

(iii) low-temperature expansion, choosing without lose of generality

$$\alpha_A > \alpha_B, \alpha_C$$

$$\Delta \simeq -\exp\left(\frac{M}{k_BT}\alpha_A^2\right)\left\{\exp\left(\frac{M}{k_BT}\alpha_B^2\right) + \exp\left(\frac{M}{k_BT}\alpha_C^2\right) - 2\exp\left(\frac{M}{k_BT}\alpha_B\alpha_C\right)\right\} \leq 0 \quad (6)$$

(iv) $\Delta < 0$ if one of the α_i's is zero, e.g., $\alpha_A > \alpha_B > \alpha_C = 0$; (v) $\Delta < 0$ if one of the α_i's lies midway between the two others:

$$\alpha_A - \alpha_B = \alpha_B - \alpha_C$$

Details on the proof of (iii)–(v) are given in the Appendix.

3. Two van der Waals Groups and a Charged Group. Suppose that group A and B interact purely via van der Waals interactions and C is a charge group. Neglecting second-order terms in $f_{CC} = u \simeq 0$ and $f_{CA} = f_{BC} = v \ll 1$, we obtain

$$\Delta = (f_{AB}^2 - f_{AA}f_{BB}) + (2v - u)(f_{AA} + f_{BB} - 2f_{AB}) \quad (7)$$

where

$$f_{ij} = \exp\left(\frac{M}{k_BT}\alpha_i\alpha_j\right), \quad \alpha_i = \alpha_A \text{ or } \alpha_B$$

For $u \simeq v \simeq 0$, the second term in (7) can be neglected and

$$\Delta \simeq \exp\left(\frac{2M}{k_BT}\alpha_A\alpha_B\right)\left\{1 - \exp\frac{M}{k_BT}(\alpha_A - \alpha_B)^2\right\} \leq 0 \quad (8)$$

From (8), we see that this case is HEC.

4. Electrostatic Interactions. Two of the three groups are oppositely charged, e.g., B positive and C negative with

$$w = f_{BC} \gg f_{BB} = f_{CC}$$

(24) Salem, L.; Chapuisat, X.; Segal, G.; Hiberty, P. C.; Minot, C.; Leforestier, C.; Sautet, P. *J. Am. Chem. Soc.* **1987**, *109*, 2887–2894.

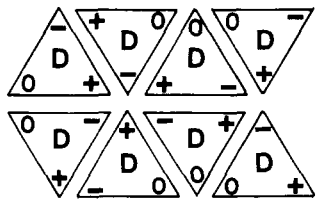

Figure 8. HOC ground-state arrangement for case 4 or section V.

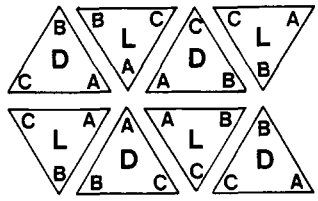

Figure 9. HEC ground-state arrangement for case 5 or section V. Nearest-neighbor groups are always the same.

If the third group is *apolar* and interacts equivalently with B and C, then

$$\Delta = (w - f_{BB})(w + f_{BB} + 2u - 4v) \tag{9}$$

where $u = f_{AA}$ and $v = f_{AB} = f_{AC}$. HOC ($\Delta > 0$) occurs as soon as

$$w > f_{BB} \quad \text{and} \quad w > 4v - 2u - f_{BB} \tag{10}$$

or

$$w < f_{BB} \quad \text{and} \quad w < 4v - 2u - f_{BB} \tag{10'}$$

However, condition 10′ cannot occur since $w = f_{BC} \gg f_{BB}$ for B and C oppositely charged. Thus, only (10) is the condition for HOC.

As a first approximation we can set $f_{BB} = 0$ and write a simplified expression for the chiral discrimination parameter:

$$\Delta \simeq w^2 + 2w(u - 2v) \tag{11}$$

As soon as $w > 2(2v - u)$, then $\Delta > 0$ (HOC).

Thus, for strong electrostatic attraction, $w \gg 1$, HOC is the preferred arrangement. The same conclusion holds if the opposite charges B and C are replaced by two *opposite dipoles* pointing in the direction perpendicular to the monolayer plane. For two oppositely charged and one neutral groups, a most likely ground-state arrangement of our tripod molecules on a hexagonal lattice is shown on Figure 8. This is an HOC arrangement with opposite charge groups as nearest neighbors.

5. Strongly Preferred Like Groups. Intermolecular interactions strongly prefer the same groups as nearest neighbors: $f_{ij} > 0$ for $i = j$, and $f_{ij} = 0$ for $i \neq j$. For this case

$$\Delta = -[f_{AA}f_{BB} + f_{BB}f_{CC} + f_{CC}f_{AA}] < 0 \tag{12}$$

clearly, a HEC case. Moreover, the ground state ($T = 0$) can be obtained by arranging the D and L enantiomers on two interpenetrating triangular sublattices, Figure 9. The D sublattice has as its nearest neighbors only sites that belong to the L sublattice and vice versa. For this HEC arrangement (similar to an antiferromagnetic ground state on a hexagonal lattice) all interactions between like enantiomers are avoided.

Another possibility is having all three like interactions AA, BB, and CC with the same weight, $f_{ii} = u$, which differs from the weight of unlike groups, $f_{ij} = v$, $i \neq j$. This is also HEC (even for $u < v$, see case 6 below) since

$$\Delta = -3(u - v)^2 < 0 \quad \text{(HEC)} \tag{13}$$

6. Strongly Preferred Unlike Groups. The opposite case of 5 occurs when only different groups can be nearest neighbors: $f_{ij} = 0$ for $i = j$ and $f_{ij} > 0$ for $i \neq j$. Calling $u = f_{AB}$, $v = f_{BC}$, and $w = f_{CA}$

$$\Delta = u^2 + v^2 + w^2 - 2uv - 2vw - 2wu \tag{14}$$

For the physically realizable quarter, $u, v, w \geq 0$, the two cases HEC and HOC are possible depending on the values of u, v, and w. The boundary, $\Delta = 0$, defines a cone of revolution in the three-dimensional parameter space (u,v,w), centered around the $u = v = w$ (111) direction. The HEC ($\Delta < 0$) region lies inside the cone while the HOC region is outside.

7. One "Passive" Group. If one of the three groups A, B, and C is "indifferent", e.g., $f_{Ai} = w$ for any i = A, B, or C

$$\Delta = (f_{BC} - w)^2 - (f_{BB} - w)(f_{CC} - w) \tag{15}$$

then both HEC and HOC cases can be obtained. In particular, if f_{BC} is larger than any of the other interactions, then $\Delta > 0$ (HOC).

VI. Phase Diagram for Chiral Monolayers: Theory

In section IV we averaged over the intermolecular interactions V_{ij} and obtained the chiral discrimination parameter Δ. This single parameter indicates whether a pair of the same enantiomers D–D or L–L interacts more or less favorably then a pair of opposite enantiomers, D–L.

A thermodynamic model can now be constructed using this chiral discrimination as an important parameter. In general, three pair interactions exist for the two species; E_{DD} and E_{LL} are the interaction energies of the pair D–D and L–L, with $E_{DD} = E_{LL}$ because of the left–right symmetry, and $E_{DL} = E_{LD}$ is the interaction of the pair D–L.

The interactions E_{ij} between molecules as a whole should be distinguished from the previously introduced interactions, V_{ij}, between the three molecular groups A, B, and C. By calculating the two-molecule partition function, we averaged over the various intermolecular group interactions V_{ij} with the proper Boltzmann factor and obtained the chiral discrimination parameter Δ. For convenience, we introduce another (but equivalent) chiral discrimination parameter

$$J = \tfrac{1}{4}(E_{DL} - E_{DD}) = \tfrac{1}{4}k_BT \log (Z_{DD}/Z_{DL}) \tag{16}$$

instead of

$$\Delta = Z_{DD} - Z_{DL}$$

Both Δ and the new chiral discrimination parameter J (eq 16) can be used interchangeably because $\Delta > 0$ (<0) if and only if $E_{DL} - E_{DD} > 0$ (<0); thus, both change sign simultaneously.

When an enantiomer mixture is studied in a Langmuir trough, the area/molecule is controlled by the surface pressure Π. To allow a variable area/molecule, we use a lattice-gas model with three components: the two enantiomers, D and L, plus *vacancies* V as a third component. The "artificial" vacancies allow us to vary the area/molecule of the "real" molecules. The three-component model D + L + V can also be used to study sublimation of bulk three-dimensional systems where V is the vapor phase, mixtures of the two enantiomers with an achiral solvent V, or with some modifications even a D + L solution with a chiral solvent.

The three area fractions (two-dimensional volume fractions) of D, L, and S are Φ_D, Φ_L, and Φ_V. The "real" area/molecule is proportional to $1/(\Phi_D + \Phi_L)$, since the three fractions add up to unity, $\Phi_D + \Phi_L + \Phi_V = 1$. In addition to the two interactions, $E_{DD} = E_{LL}$ and E_{DL}, between D and L, two other interactions describe the interactions with V: $E_{DV} = E_{LV}$ and E_{VV}.

The free energy of the three-component system is $F = E - TS^{mix}$, where E is the internal energy and S^{mix} is the entropy of mixing of the three components:

$$S^{mix} = -k_B(\Phi_D \log \Phi_D + \Phi_L \log \Phi_L + \Phi_V \log \Phi_V) \tag{17}$$

$$E = \tfrac{1}{2}\Phi_D^2E_{DD} + \tfrac{1}{2}\Phi_L^2E_{LL} + \Phi_D\Phi_LE_{DL} + \tfrac{1}{2}\Phi_V^2E_{VV} + \Phi_D\Phi_VE_{DV} + \Phi_L\Phi_VE_{LV} \tag{18}$$

Equation 18 includes the most general pairwise interactions between D, L, and V. From (17) and (18), $F = E - TS^{mix}$ is the free energy within mean-field approximation for the three-component system. In (18) there are four independent interactions E_{ij} and two independent area fractions (densities) Φ_i. A similar expression for F has been introduced by Schipper and Harrowell[25]

to compare solubilities of D and L enantiomers in a chiral solvent.

The following reduced densities are introduced for convenience:

$$Q = \Phi_D + \Phi_L = 1 - \Phi_V \quad (19)$$

which is proportional to the monolayer coverage and

$$M = \Phi_D - \Phi_L \quad (20)$$

The densities M and Q are related to the experimentally controlled D/L mole fraction: $x = (1 - M/Q)/2$.

The internal energy E can be written as a function of M and Q. Since linear terms in E can be absorbed in the definition of the chemical potentials (see below), E has the following quadratic form:

$$E = -KQ^2 - JM^2 \quad (21)$$

with

$$K \equiv -\tfrac{1}{4}(E_{DD} + E_{DL} + 2E_{VV} - 4E_{DV})$$
$$J \equiv \tfrac{1}{4}(E_{DL} - E_{DD}) \quad (22)$$

The parameter K measures the tendency of the system as a whole to condense, whereas J is equal to the chiral discrimination (16); $J > 0$ is homochiral (HOC), $J < 0$ is heterochiral (HEC), and $J = 0$ if and only if $\Delta = 0$ (no chiral discrimination).

The convexity of the free energy F as a function of Q and M, (17)–(22), determines the phase behavior:

$$F(Q,M) = -KQ^2 - JM^2 - TS^{mix} \quad (23)$$

with

$$S^{mix} = -k_B[\tfrac{1}{2}(Q + M)\log(Q + M) + \tfrac{1}{2}(Q - M)\log(Q - M) + (1 - Q)\log(1 - Q) - Q\log 2] \quad (24)$$

Nonconvex regions of $F(Q,M)$ are multiphase regions. A common tangent construction indicates the extent of such multiphase regions. Alternatively, we look for coexistence of the minima of

$$G = F - DQ - HM \quad (25)$$

with respect to Q and M, where D and H are the two conjugated fields (chemical potentials) to Q and M, respectively. Notice that all linear terms omitted in (21) can be absorbed in the two fields D and H.

The minima of G satisfy the following equations:

$$\left.\frac{\partial G}{\partial Q}\right|_M = 0 \qquad \left.\frac{\partial G}{\partial M}\right|_Q = 0$$

leading to

$$D(Q,M) = -2KQ + k_BT[\tfrac{1}{2}\log(Q^2 - M^2) - \log(1 - Q) - \log 2] \quad (26)$$

$$H(Q,M) = -2JM + \tfrac{1}{2}k_BT\log\left(\frac{Q + M}{Q - M}\right) \quad (27)$$

For given energy parameters J and K and a given temperature T, the two-order parameters Q and M depend on the two fields D and H. In general, the transcendental equations (26) and (27) have to be solved numerically. Several minima of G for a given D and H indicate multiphase regions. The value of the free energy at its minimum, $G = G_e$, can be obtained by substituting $D(Q,M)$ and $H(Q,M)$ from (26) and (27) into the general expression for G, (23)–(25):

$$G_e(Q,M) = KQ^2 + JM^2 + k_BT\log(1 - Q) \quad (28)$$

Using the relationship between the pressure Π and the equilibrium free energy for lattice-gas models[26,27]

$$\Pi = -G_e = -KQ^2 - JM^2 - k_BT\log(1 - Q) \quad (29)$$

several theoretical phase diagrams involving the surface pressure can be calculated. Fixing the material-dependent energy parameters J and K, one plots isotherms, i.e., the variation of the surface pressure Π with the area/molecule or with $Q = \Phi_D + \Phi_L$, for fixed temperature. Two other useful plots are (i) Π–x diagram for a fixed temperature and (ii) Π–T diagram for a fixed D/L mole fraction x.

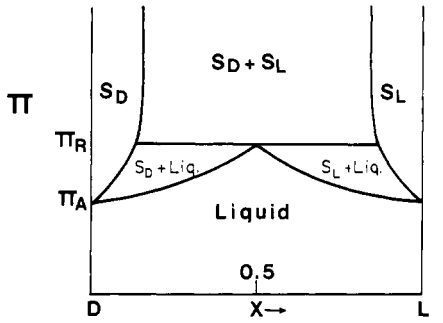

Figure 10. Schematic phase diagram of the transition pressure Π_c as a function of the racemic composition x, for a fixed temperature, calculated from (23)–(29), for J, $K > 0$ and $k_BT/J < 2.95$. Compare with sublimation of conglomerates, Figure 2a.

It can be shown that our free-energy formulation for the D + L + V chiral mixture, (26) and (27), is identical with the mean-field approximation of a general three-component liquid mixtures, extensively studied within the framework of *Blume–Emery–Griffiths* (BEG) spin-1 model.[27-32] In the BEG model, a spin variable having three degrees of freedom ($S_i = -1, 0, 1$) for the three liquid components is assigned to each site of the lattice. For chiral monolayers, $S_i = +1, -1, 0$, is a site occupied by D, L, or an empty site (vacancy), respectively. The BEG model has the following Hamiltonian:

$$-\mathcal{H} = J\sum_{\langle i,j\rangle} S_iS_j + K\sum_{\langle i,j\rangle} S_i^2S_j^2 + H\sum_i S_i + D\sum_i S_i^2 \quad (30)$$

where the sum $\langle i,j\rangle$ is over nearest-neighbor sites of the lattice and is a generalization of a lattice-gas model[26] with $S_i = 0$ or 1, used to study two-component systems such as liquid–gas or binary liquid mixtures. Therefore, we make use of previously calculated[27] phase diagrams for the BEG model (within mean field) for chiral mixtures.

In Figure 10, the Π–x phase diagram is plotted schematically for the homochiral case (HOC), J, $K > 0$ and low temperatures, $0 < k_BT/J < 2.95$, $J/K \simeq 1/3$. The exact phase diagram can be found in ref 27c. For this range of temperatures, the model gives essentially a conglomerate phase diagram as was explained in section III. The three phases, liquid (liq), D solid (S_D), and L solid (S_L) are separated by three two-phase regions: liq + S_D, liq + S_L, and S_D + S_L. This is very similar to the actual conglomerate phase diagram presented in Figure 2a.

The main difference between the calculated and experimental phase diagrams, Figures 10 and 2a, is the extent of the "pure" enantiomeric solid in Figure 10, namely, the existence of a solid solution in the vicinity of the pure enantiomers D and L. Such phase diagrams are characteristic of chiral mixtures called *pseudoracemates*.[33] However, to understand it theoretically, we recall that the BEG model is appropriate for liquid mixtures or liquid–gas transitions. As for any lattice–gas model, it is less appropriate to describe solidification. Only for very low temperatures, the extent of the single solid phases shrinks to zero, and the phase diagram then looks exactly like that for a true conglomerate. Another complication occurs at higher tempera-

(25) Schipper, P. E.; Harrowell, P. R. *J. Am. Chem. Soc.* **1983**, *105*, 723–730.
(26) (a) Temperley, H. N. V. *Proc. Phys. Soc. (London)* **1954**, *A67*, 233. (b) Lee, T. D.; Yang, C. N. *Phys. Rev.* **1952**, *87*, 410.
(27) (a) Sivardière, J.; Lajzerowicz, J. *J. Phys. Rev. A* **1975**, *11*, 2079–2089. (b) *Ibid.* **1975**, *11*, 2090–2100. (c) *Ibid.* **1975**, *11*, 2101–2110.
(28) Blume, M.; Emery, V. J.; Griffiths, R. B. *Phys. Rev. A* **1971**, *4*, 1071–1077.
(29) Mukamel, D.; Blume, M. *Phys. Rev. A* **1974**, *10*, 610–617.
(30) Furman, D.; Dattagupta, S.; Griffiths, R. B. *Phys. Rev. B* **1977**, *15*, 441–464.
(31) Berker, A. N.; Wortis, M. *Phys. Rev. B* **1976**, *14*, 4946–4963.
(32) A general three-component mixture has also a cross Q·M term in the free energy. For enantiomer mixtures, such a term is always zero because of the left–right symmetry.
(33) See Chapter 2.4 in ref 2.

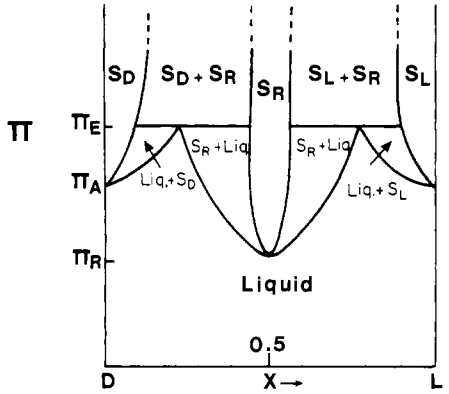

Figure 11. Expected phase diagram of Π_c as function of x, from (23)–(29), for $J < 0$ and $K > 0$. Compare with sublimation of racemates, Figure 2b.

tures: $k_BT/J > 2.95$, where the model predicts multicritical phenomena (critical and tricritical points) that have never been observed in solidification of enantiomer mixtures.

For the heterochiral case (HEC), $K > 0$ and $J > 0$, a more complicated treatment is needed even on a mean-field level. It is not enough to look for the solution of (26)–(28) with $J < 0$. As for binary alloys (β-brass), the two possible "antiferromagnetic" order parameters have to be allowed. Instead of the two order parameters M and Q, we will have three: the coverage Q as before, but two enantiomeric compositions—one on sublattice A, $M_A = \langle S_A \rangle$, and the second on sublattice B, $M_B = \langle S_B \rangle$. The detailed phase diagrams will be presented elsewhere. We expect them to show also a pseudoracemate behavior, where pure enantiomeric solids S_D and S_L as well as the racemate solid S_R extend over a finite range of racemic compositions. Otherwise, the expected phase behavior shown schematically in Figure 11 is quite similar to the actual racemic compound behavior, Figure 2b.

VII. Discussion

In section V, we discussed the chiral discrimination for several particular types of interactions. For simplicity, only two nearest-neighbor interactions have been taken into account, and a Boltzmann-weighted average has been performed on the nine "back-to-back" relative orientations of a pair of tripod molecules.

In particular, we would like to note the difference between van der Waals (case 2) and electrostatic (case 4) interactions. For the former, a HEC behavior is predicted, whereas the latter is HOC. For most of the other cases, chiral discrimination depends more closely on the relative strength of the various V_{ij} interactions, and no general conclusion is possible.

Another chiral molecular arrangement worth mentioning is an asymmetric carbon connected to *three different polar or charge groups* and to an aliphatic tail. This proposed molecule is an amphiphile and has two stereomeric arrangements, D and L. To the best of our knowledge such a chiral amphiphile has not been studied for its chiral discrimination. Theoretically, treating the case of three charges or dipolar groups is rather complicated (frustration effects), in contrast to tripods with only two opposite charges discussed in section V. Strong competition between electrostatic interactions can lead to complex crystalline order even for the two-dimensional monolayer geometry. Our simple model, which averages over all intermolecular interactions and predicts a single parameter—the chiral discrimination—is probably less suitable for this case.

In section VI, we presented a thermodynamical model that predicts qualitatively some of the features of a monolayer phase diagram. A three-component model is used to mimic the variable area per molecule of chiral amphiphilic monolayers. The molecular interaction parameters E_{ij} depend crucially on the chiral discrimination. Generalizations of this model can describe solutions of enantiomer mixtures as well as sublimation of bulk enantiomer mixtures.

Most of the important features of conglomerate phase diagrams are reproduced theoretically, Figure 10, although the final extent of the "pure" D and L solids is an artifact (pseudoracemate behavior). For racemic compounds, the study of the phase diagram is more complex, but from preliminary studies we expect a qualitative agreement with experiments (cf. Figures 2b and 11). We also note that the mean-field approximation employed here does not predict correctly all the features of the two-dimensional critical behavior. Critical fluctuations should be included in future calculations.[31] On the other hand, our mean-field phase diagrams can also be applied to explain three-dimensional sublimation or solutions of chiral mixtures.

VIII. Applications and Connection with Experiments

Is it possible to compare our predictions to available experimental data on chiral monolayers? Unfortunately, at present the answer is no. The main problem is that, in past experiments, chiral monolayers did not have the simple tripod structure. In some cases, the amphiphiles even have two chiral centers. Another important issue, even with one chiral center, is the need to attach to the chiral carbon three groups that will lie on the water/air interface.

Nevertheless, the various cases discussed earlier can be realized in experiments even if the affinity to the water/air interface is caused only by one or two groups, provided that the molecule behaves as an "effective" tripod, i.e., its molecular orientations include mainly rotation of the tripodal base on the water surface. Our general consideration of the various types of molecular interactions, charges, dipoles, and van der Waals, can be tested, at least qualitatively, by designing new chiral tripods.

Another possible setup to test chiral discrimination in monolayers is the adsorption of a chiral monolayer on a graphite surface or the use of chiral molecules in graphite intercalation compounds.[34] If a physioadsorption is carried out so that *always* the same three of the four molecular groups lie on the graphite surface, chiral discrimination can play an important role.[35] However, an additional complication of adsorption on solid surfaces such as graphite is the existence of preferred adsorption sites. The solid surface cannot be regarded only as a passive support. Rather, the interactions of the surface with the chiral molecules can influence the two-dimensional ordering of the monolayer.

Finally, we note that a promising future experiment, in our opinion, may be a simultaneous comparison between epifluorescence microscopy and a detailed monolayer isothermal investigation for the same material. As a first step, it will be even interesting to observe the chiral pattern formation (or the lack of it) as a function of enantiomeric composition for certain phospholipids where chiral domains have been seen for pure enantiomers and for some 1:1 D + L mixtures.[4-7] Will a 1:1 D + L mixture show *achiral* domains or the two types of *chiral* domains side by side? The two are possible and depend on the chiral discrimination.

As a continuation, a comparison with the monolayer phase diagrams can follow and could greatly enhance our understanding of chiral discrimination in monolayers. We hope that the present study will motivate such experimental investigations. One possible difficulty to tackle is to find chiral amphiphiles that on one hand can be used in epifluorescence microscopy and on the other hand have a measurable variation in the transition pressure (bigger than a few dyn/cm) as the enantiomer composition is varied.

Acknowledgment. I thank P.-G. de Gennes for introducing me to the subject of chiral systems and for many helpful suggestions and comments. Certain results for tripod amphiphiles have been previously reported by P.-G. de Gennes and the author in a short note (ref 8). It also thank J. M. di Meglio, J. Jacques, H. Kagan, J. Lajzerowicz, H. M. McConnell, H. Möhwald, E. Raphael, M. Schick, J. Sivardière, B. Widon, and especially A. Collet and M. Dvolaitzky for comments and correspondence. The support of

(34) I thank H. Kagan for this suggestion. Segregation of enantiomers of chiral complexes in montmorillonites has been studied: Joshi, V.; Kotkar, D.; Gosh, P. K. *J. Am. Chem. Soc.* **1985**, *108*, 4650–4651.

(35) Adsorption of chiral molecules onto a triangular lattice has been studied: (a) Huckaby, D. A.; Ausloos, M.; Clippe, P. *J. Chem. Phys.* **1985**, *82*, 5140–5145. (b) Huckaby, D. A.; Shinmi, M.; Ausloos, M.; Clippe, P. *J. Chem. Phys.* **1986**, *84*, 5090–5094.

the U.S.-Israel Binational Science Foundation under Grant 87-00338, the Bat Sheva de Rothschild Foundation, and Exxon Research and Engineering Co. is gratefully acknowledged.

Appendix

The proof of the inequalities used for van der Waals interactions, section V, is presented here.

(a) To show that $\Delta < 0$ in the low-temperature expansion (6), we recall that for any $x \neq y$

$$\exp(x^2) + \exp(y^2) - 2\exp(xy) > 2\exp(\tfrac{1}{2}x^2 + \tfrac{1}{2}y^2) > 0 \quad \text{(A1)}$$

where the convexity of the exponential function is used in (A1); the HEC inequality in (6) immediately follows.

(b) For case iv of section V, one of the α_i's is zero while the other two are positive. For example, $\alpha_A > \alpha_B > \alpha_C = 0$. Using the expression for Δ from (3) and (4) with

$$x^2 = \frac{M}{k_B T}\alpha_A^2 \qquad y^2 = \frac{M}{k_B T}\alpha_B^2$$

we get[36]

$$\Delta = e^{2xy} - e^{x^2+y^2} + e^{x^2} + e^{y^2} - 2e^{xy} = (e^{xy} - 1)^2 - (e^{x^2} - 1)(e^{y^2} - 1) \quad \text{(A2)}$$

since the function $f(u) = \log(e^{e^u} - 1)$ is convex

$$f(u_A) + f(u_B) > 2f(\tfrac{1}{2}u_A + \tfrac{1}{2}u_B) \quad \text{(A3)}$$

Substituting $u_A = 2\log(x)$, $u_B = 2\log(y)$, we have from (A3)

$$\log(e^{x^2} - 1) + \log(e^{y^2} - 1) > 2\log(e^{xy} - 1) \quad \text{(A4)}$$

Thus, $\Delta < 0$ in (A2).

(36) De Gennes, P.-G., private communication.

(c) For case v of section V, α_B lies midway between α_A and α_C:

$$\alpha_B = \alpha_C + \delta = \alpha_A - \delta \quad \text{(A5)}$$

Define

$$u = \exp\left(\frac{M}{k_B T}\alpha_B\delta\right) \qquad v = \exp\left(\frac{M}{k_B T}\delta^2\right)$$

From (3)

$$\Delta = u^{-2}v^{-2}(v-1)[2uv(v+1) - 2uv^2 + 2u^3v(v+1) - u^4v^2 - v^2 - u^2(1 + v + v^2 + v^3)] \quad \text{(A6)}$$

$P(u,v) = -\Delta u^2v^2/(v-1)$ is a third-degree polynomial in v. A Taylor expansion around $v = 1$ contains four terms:

$$P(u,v) = P(u,1) + (v-1)\frac{\partial P(u,1)}{\partial v} + \frac{1}{2}(v-1)^2\frac{\partial^2 P(u,1)}{\partial v^2} + \frac{1}{6}(v-1)^3\frac{\partial^3 P(u,1)}{\partial v^3} \quad \text{(A7)}$$

where

$$P(u,1) = (u-1)^4 > 0 \quad \text{(A8)}$$

$$\frac{\partial P(u,1)}{\partial v} = 2(u-1)^2(u^2 - u + 1) > 0 \quad \text{(A9)}$$

$$\frac{\partial^2 P(u,1)}{\partial v^2} = 2(u^4 - 2u^3 + 4u^2 - 2u + 1) > 0 \quad \text{(A10)}$$

$$\frac{\partial^3 P(u,1)}{\partial v^3} = 6u^2 > 0 \quad \text{(A11)}$$

Since $P^{(n)}(u,1) > 0$ for $3 \geq n \geq 0$, then $P(u,v) > 0$ for all $v > 1$. In other words, from (A7)-(A11), $\Delta < 0$ (HEC).

Relative Ring-Current Effects Based on a New Model for Aromatic-Solvent-Induced Shift[1]

Helmut Stamm* and Hannelore Jäckel

Contribution from the Pharmazeutisch-Chemisches Institut der Universität Heidelberg, Im Neuenheimer Feld 364, D-6900 Heidelberg, Federal Republic of Germany.
Received January 2, 1986

Abstract: A convenient method for measuring (relative to benzene) the above-plane ring-current effect of aromatic compounds is presented. The method is based on strictly linear relations $\Delta_{oi} = (\bar{a} + b)[D_o]_i$ between the induced upfield shift Δ_{oi} of an (externally referenced) ^{1}H NMR signal of a probe and the concentration $[D_o]_i$ of the aromatic D (solvent CCl_4). Δ_{oi} is the chemical shift relative to that of the solution where $[D_o]_i = 0$, and b is the necessary correction for the change in the susceptibility. A study of more than 30 compounds D (including the partial antiaromatic biphenylene) with 1-chloroisobutene as probe shows that its $\bar{a}$ values establish a relative scale of the above-plane ring-current effect. This relative scale generally displays a good agreement with a similar scale derived from diamagnetic exaltations. The probe behavior is explained by a simple model for ASIS (aromatic-solvent-induced shift) that divides ASIS into three components: upfield contributions from AUS effects (additional nonspecific shielding effects) and from complexation, counteracted by the downfield contribution through AUS effects on the customary internal reference. The AUS effect in its most simple mode depends linearly on the concentration $[D_o]_i$ of benzene (or other aromatic compounds). Prerequisites for the linear dependence are discussed.

Previous studies[2] of solvent (or cosolvent or cosolute) dependence of ^{1}H NMR chemical shifts δ have usually compared chemical shifts of the solute at a more or less constant concentration. In some studies the chemical shifts δ were extrapolated to zero solute concentration. To the best of our knowledge, however, a comparison of *slopes* of *linear* shift-concentration relations, obtained from constant solute concentration as a function of the much larger concentrations of a cosolvent or cosolute, have not yet been reported. Such linear relations over a large concentration range in high-precision experiments have seldom been observed before and never for a whole series of cosolvents or cosolutes. This paper reports now on such a unique behavior and on its relation to the so-called ring-current effect. An explanation of the observed linear relation is presented on the basis of a new model for ASIS, the

(1) Dedicated to the memory of Professor Hans Musso.

(2) Laszlo, P. In *Progress in Nuclear Magnetic Resonance Spectroscopy*; Emsley, W., Feeney, J., Sutcliffe, L., Eds.; Pergamon Press: Oxford 1967; Vol. 3, Chapter 6, pp 231-402. Ronayne, J.; Williams, D. H. In *Annual Review of NMR Spectroscopy*; Mooney, E. F., Ed.; Academic Press: London, 1969; Vol. 2, pp 83-124.

0002-7863/89/1511-6544$01.50/0